small methods
www.small-methods.com

Flexible Stretchable Piezoelectric Films for Tissue Repair and Health Detection

Yujie Xiong, Ruizeng Luo, Yilin Qi, Longfei Li, Qiao Yu, Yuan Bai, Lingling Xu, Xiong Guo, Xi Cui, Haochen Xie, Weina Li, Daidi Fan,* Hongyu Meng,* and Zhou Li**

In the context of deepening interdisciplinary research and increasing public health awareness, self-powered technology based on piezoelectric materials has gradually attracted attention in the field of health monitoring and treatment owing to its wireless and passive nature. Sustainable development has prompted the development of degradable piezoelectric materials. However, most degradable piezoelectric materials cannot be applied to active parts of the human body because of their poor strain capacity and toughness. In this study, based on poly (L-lactic acid) (PLLA) and recombinant human type I collagen (Col I), a biodegradable, stretchable d-PLLA/Col piezoelectric film is prepared using electrospinning technology. Cross-linked Col I provides d-PLLA/Col with better flexibility and stretchability, which can adapt to low-frequency tissue deformation or activity, thus improving fit stability and electromechanical sensing performance in wearable applications. Furthermore, under a high-frequency ultrasonic drive, electrical stimulation generated by d-PLLA/Col synergistically promotes wound healing in rats with a biomimetic extracellular matrix and structure. This study provides new insights into the development of degradable piezoelectric materials and offers a feasible strategy for next-generation health diagnostic and treatment devices.

1. Introduction

Flexible electronics have emerged as promising solutions for therapeutic and health monitoring applications.[1–4] The combination of flexible electronics and self-powered technologies has resulted in lightweight and comfortable devices that do not require external power and can monitor and intelligently provide a patient's physiological status in real time for health diagnosis and treatment.[5,6] Self-powered technology based on piezoelectric materials, which generate electrical charges under mechanical deformation and convert mechanical energy into electrical energy, are vital for the development of health monitoring and therapeutic devices.[7–10] However, conventional nonbiodegradable piezoelectric materials, such as lead zirconate titanate ceramics, pose significant challenges owing to their poor biosafety and the potential environmental risks associated with their production and disposal.[11,12] In response, biodegradable bio-piezoelectric materials have gained significant attention due to their superior biosafety and biodegradability.[13,14]

Degradable bio-piezoelectric materials are typically classified into two categories: small-molecule, crystal-based materials (e.g., amino acids and short peptides) and polymer-based materials.[15,16] While small molecule piezoelectric materials, including amino acids, are often brittle and difficult to adapt for flexible applications,[15] polymer-based degradable piezoelectric materials generally exhibit greater flexibility.[17,18] Among these, poly(L-lactic acid) (PLLA) has emerged as a leading biopolymer owing to its exceptional piezoelectric properties, flexibility, and processability.[19]

Y. Xiong, W. Li, D. Fan
Engineering Research Center of Western Resource Innovation Medicine Green Manufacturing
Ministry of Education
School of Chemical Engineering
Northwest University
Xi'an 710127, China
E-mail: 20154798@nwu.edu.cn; fandaidi@nwu.edu.cn

Y. Xiong, R. Luo, Y. Qi, L. Li, Q. Yu, Y. Bai, L. Xu, X. Guo, X. Cui, H. Xie, H. Meng
Beijing Institute of Nanoenergy and Nanosystems
Chinese Academy of Sciences
Beijing 101400, China
E-mail: menghy@iccas.cas.cn

The ORCID identification number(s) for the author(s) of this article can be found under https://doi.org/10.1002/smtd.202500247

DOI: 10.1002/smtd.202500247

Z. Li
Tsinghua Changgung Hospital
School of Clinical Medicine
Tsinghua University
Beijing 100084, China
E-mail: li_zhou@tsinghua.edu.cn

Z. Li
School of Biomedical Engineering
Tsinghua University
Beijing 100084, China

Y. Xiong, W. Li, D. Fan
Shaanxi Key Laboratory of Degradable Biomedical Materials and Shaanxi R&D Center of Biomaterials and Fermentation Engineering
School of Chemical Engineering
Northwest University
Xi'an 710127, China

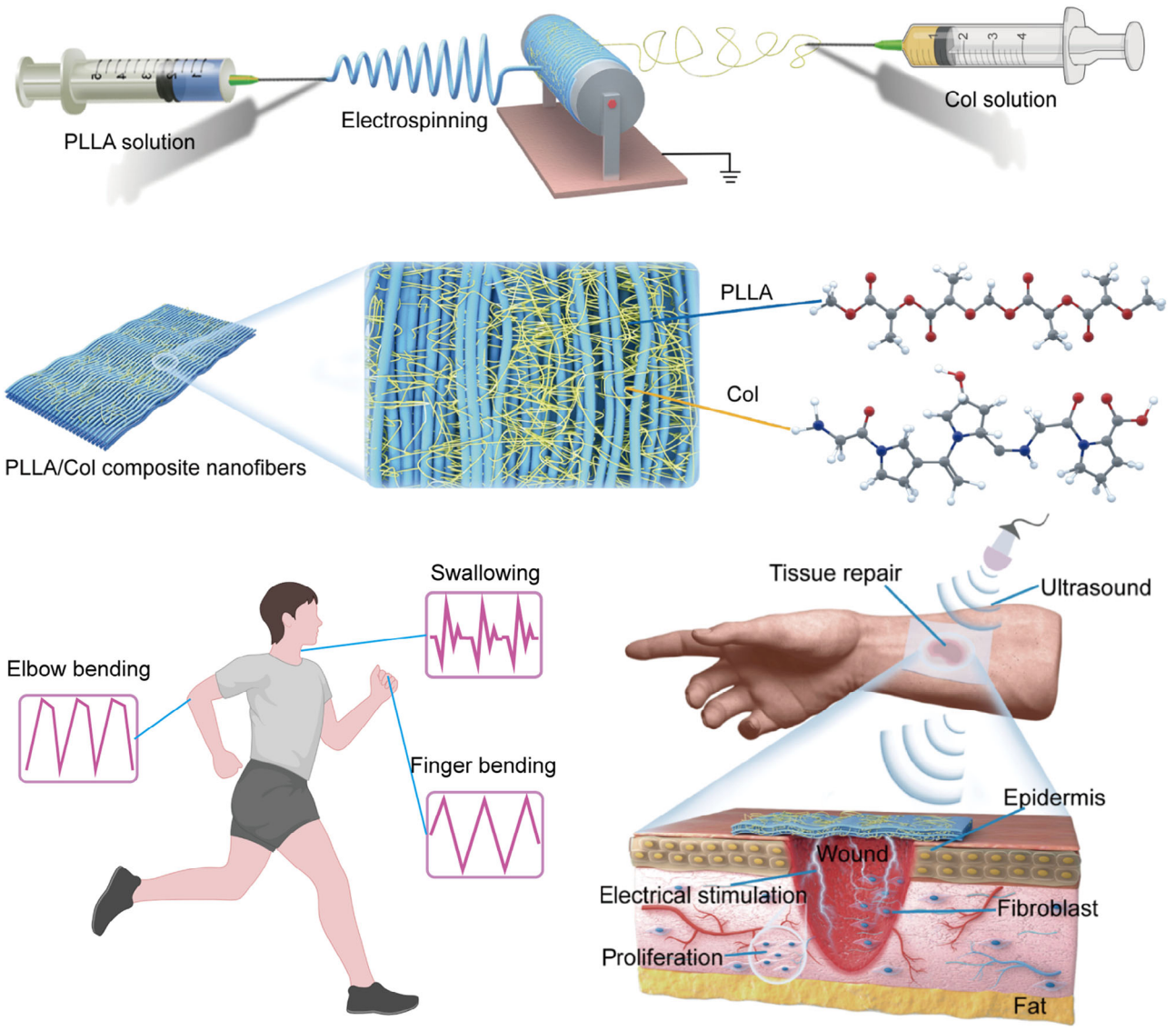

Figure 1. PLLA and recombinant collagen composite film preparation process and application demonstration.

Electrospinning further enhances the piezoelectricity and flexibility of PLLA by optimizing its mechanical and electrical properties, thereby broadening its applicability in health monitoring and tissue repair.[20] For tissue repair, a single electrical stimulation treatment may not always yield optimal results. To address this, recombinant humanized type I collagen has been incorporated as it has been shown to be effective in tissue regeneration.[21,22] As a key component of the extracellular matrix, recombinant collagen promotes cell attachment and proliferation, whereas the humanized version reduces the risks of immune rejection and pathogen transmission associated with animal-derived collagen.[23,24] The interfacial interaction between recombinant collagen and PLLA, along with the cross-linking of collagen, further enhances the mechanical properties of the film, including flexibility and tensile strength. This synergy accelerates tissue repair and expands the potential applications of this material for wearable health detection, highlighting its promising prospects.

This paper presents a flexible and stretchable piezoelectric film fabricated via electrospinning that is suitable for wound repair and health monitoring (**Figure 1**). Composed of PLLA and recombinant collagen, the composite membrane scaffold features uniformly dispersed nanofibers achieved through a two-tube composite spinning process. The physicochemical properties of the PLLA-recombinant collagen scaffold, such as its morphology, hydrophilicity, electrical output, and mechanical strength, were comprehensively characterized. The potential of the film for in vitro health monitoring was also explored, along with an evaluation of its biocompatibility and the directed growth and proliferation of cells on the scaffolds. Furthermore, the synergistic effects of PLLA-recombinant collagen scaffolds on tissue repair were assessed in a rat whole-skin wound model.

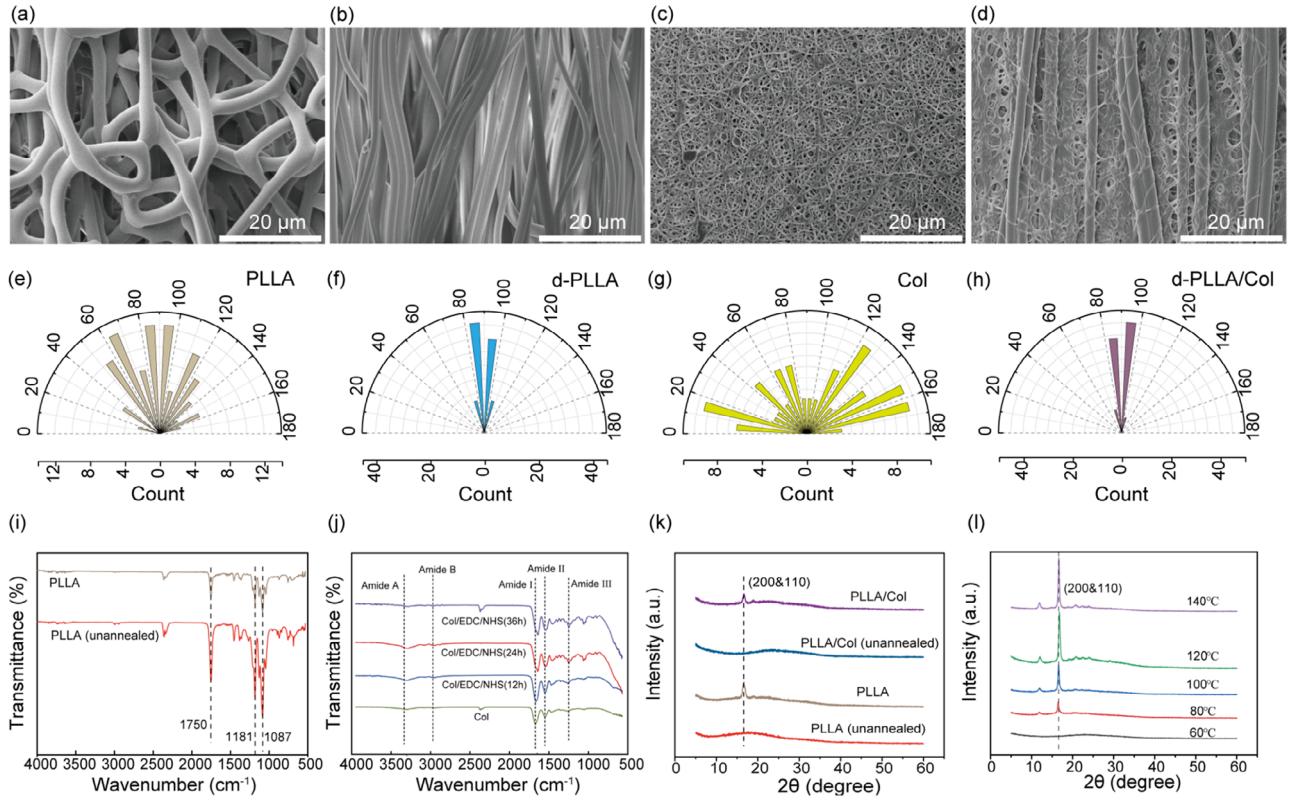

Figure 2. Scanning electron microscopy images of the surface morphology of a) PLLA, b) d-PLLA, c) Col, and d) d-PLLA/Col films. e–h) Nanofiber orientations of PLLA, d-PLLA, Col, and d-PLLA/Col films, with 0° being perpendicular to the direction of the receiver rotation. i) ATR-FTIR spectra of PLLA and unannealed PLLA. j) ATR-FTIR spectra of Col with different cross-linking times. k) XRD patterns of PLLA, unannealed PLLA, PLLA/Col, and unannealed PLLA/Col. l) XRD patterns of PLLA/Col at various annealing temperatures.

2. Results and Discussion

2.1. Preparation and Characterization of PLLA/Col Nanofiber Film Scaffolds

Electrospinning has been widely used in the preparation of nanofiber films owing to its simple operation and excellent tunability of the material structure.[25] By adjusting the rotational speed of the electrostatic spinning collector, the coarseness and orientation of the fibers can be controlled to meet the needs of different applications.[26,27] Directed PLLA nanofibers, which can provide excellent electrical output, have also shown advantages in tissue repair applications.[28] **Figure** 2a–d depicts the microscopic morphologies of the annealed PLLA films at 500 and 2500 rpm, cross-linked Col films at 2500 rpm, and cross-linked annealed PLLA/collagen (d-PLLA/Col) composite nanofiber films at 2500 rpm. These were referred to as PLLA, d-PLLA, Col, and d-PLLA/Col, respectively. For better comparison, the morphologies of the unannealed films at 500 rpm for PLLA, 2500 rpm for PLLA, 2500 rpm for Col, and 2500 rpm for PLLA/Col composite nanofibers without annealing or cross-linking treatments are shown in Figure S1 (Supporting Information). To visualize the orientation of the electrospun nanofibers, the distribution angle of the fibers at different collector rotational speeds was quantified using microscopic morphology maps, as shown in Figure 2e,f and Figure S2 (Supporting Information). At 500 rpm, the fiber distribution in the 70°–110° range accounted for 37.5%, whereas the fiber angle distribution in the 80°–100° range was 25%. At 2500 rpm, the fiber distribution in the 70°–110° range reached 100%, with 75% of the fiber angles concentrated in the 80°–100° range. In addition, at an intermediate rotational speed (1000 rpm), as shown in Figure S3 (Supporting Information), the fiber films showed significant improvements in both orientation and alignment compared to those prepared at 500 rpm, whereas the films prepared at 2500 rpm showed further improvements in both orientation and alignment, thus verifying that higher spinning speeds can improve fiber alignment. This result aligns with the expectation that higher rotational speeds during electrospinning increase the mechanical stretching force on the fibers prior to deposition, thereby promoting elongation and better alignment. Furthermore, the fast-rotating receiver helped to align the fibers consistently along the rotational direction, thereby reducing the chances of fiber crossing and tangling. This not only improved the orientation of the fibers but also enhanced the uniformity and mechanical properties of the resulting fiber film. Despite the increased speed, the Col fiber membrane still displayed an irregular orientation at 2500 rpm, as shown in Figure 2g. This irregularity arises primarily from the low inertia and mass of the Col fibers, making them more susceptible to random motion in air, which complicates the effective orientation through receiver rotation. Additionally, electrostatic charges on the fiber surface may cause

repulsion between the fibers, especially for finer fibers, further impeding alignment. By contrast, after electrostatic spinning, the d-PLLA/Col fiber membrane retained a high degree of orientation, with the fiber distribution angle consistently concentrated between 80° and 100° (Figure 2h). These results suggest that the d-PLLA/Col fiber films exhibited excellent morphological characteristics, spatial structure, and superior fiber alignment.

The diameter range of the nanofibers is shown in Figure S4 (Supporting Information). The difference in fiber diameters between the d-PLLA and PLLA fibers can be attributed to the high rotational speed of the receiver during the electrospinning process, which induces a strong traction force on the deposited fibers. This force pulls the undeposited fibers onto the receiver, resulting in finer d-PLLA fibers than those of PLLA. Meanwhile, the EDS of d-PLLA/Col (Figure S5, Supporting Information) indicates that Col was uniformly doped with PLLA.

Fourier-transform infrared (FTIR) spectroscopy was used to analyze the chemical composition of the PLLA nanofiber scaffolds (Figure 2i). The FTIR spectrum of pure PLLA exhibited a distinctive peak at 1750 cm^{-1}, corresponding to the symmetric elongation of the ester group (υsC═O). The 1181 cm^{-1} band observed for PLLA was assigned to the asymmetric C—O—C stretching mode of the ester groups.[29] Importantly, the FTIR spectra of both annealed and non-annealed PLLA showed no shifts, confirming that both types of PLLA nanofiber scaffolds share the same chemical composition. Collagen is a water-soluble material that requires cross-linking prior to implantation. The cross-linking states were analyzed using FTIR spectroscopy. The corresponding reaction schemes and FTIR spectra are shown in Figure 2j and Figure S6 (Supporting Information). The EDC/NHS-mediated cross-linking reaction proceeds through covalent amide bond (—CONH—) formation between the carboxyl (—COOH) and amino (—NH_2) groups of collagen (Figure S6, Supporting Information).[30] The infrared spectra in Figure 2j display five characteristic bands corresponding to amides A, B, I, II, and III for both Col (uncrosslinked) and Col, indicating that the basic molecular structure remained intact. For uncrosslinked collagen, the main peak of its amide I band was located at ≈1655 cm^{-1} (dominated by the α-helix structure). After 12 h of cross-linking, its peak position was offset to 1648 cm^{-1} as the β-sheet structure was increased, and cross-linking leads to a more orderly arrangement of molecular chains. As the cross-linking time increased to 24 h, the degree of cross-linking increased, and its β-sheet structure was further increased, resulting in the main peak of the amide I band being shifted to 1630 cm^{-1}. When the cross-linking time was extended to 36 h, the position of the amide I band was essentially the same as that observed after 24 h. This indicates that the degree of cross-linking was almost the same for these two periods. Moreover, after cross-linking, the absorbance of the amide II band was enhanced, and the intensity ratio (Amide II/Amide I) increased, with larger ratios indicating a higher degree of cross-linking. A redshift in amide II was also observed after the EDC/NHS treatment, which was associated with the coupling of the N—H bending vibration and the C—N stretching vibration, further confirming the enhancement of hydrogen bonding.[31] After 24 and 36 h of cross-linking, these values were almost identical. These findings confirmed that the recombinant collagen membranes were successfully cross-linked and had a good degree of cross-linking after 24 h of cross-linking. For PLLA nanofibers, the β-form crystalline structure and crystallinity are key parameters influencing piezoelectric performance.[32] To assess these properties, 1D XRD analysis was performed on the film scaffolds, and the results are shown in Figure 2k,l. Upon post-annealing, both PLLA and PLLA/Col films exhibited peaks at the (200) and (110) planes, indicating the presence of a β-form structure and confirming their piezoelectric properties. An investigation of the annealing temperature gradient for PLLA/Col films revealed that increasing the annealing temperature enhanced crystallinity, demonstrating similar peak intensities at 120 and 140 °C and suggesting a small difference in crystallinity. Many studies have confirmed that high annealing temperatures impair the mechanical properties of PLLA materials. Increasing the annealing temperature to ≥ 115 °C resulted in a slight increase in the piezoelectric coefficient but a significant decrease in the elongation at break.[33] Based on the results of these studies and considering energy and resource efficiency, an annealing temperature of 120 °C is optimal. The necessity of annealing the nanofiber thin-film material was confirmed, and an optimal annealing temperature of 120 °C was determined.

In addition, the swelling rates of the scaffolds were measured to quantify their hygroscopicity. The results are shown in Figure S7 (Supporting Information). Swelling rate measurements indicated that the respective water absorptions of PLLA and d-PLLA were ≈15.23% and 16.14% of their respective masses. By contrast, the water absorption of PLLA/Col and d-PLLA/Col, which contained recombinant collagen, reached 124.79% and 120.89% of their masses, respectively, which were significantly higher than that of PLLA alone. The excellent hygroscopicity of the d-PLLA/Col films was further confirmed by swelling experiments. The d-PLLA/Col film effectively absorbed moisture from the wound, preventing cellular hypoxia and excessive fluid accumulation, thereby promoting efficient wound healing.[34] Additionally, the enhanced hygroscopicity significantly improved the extensibility and flexibility of the material.

2.2. Mechanical and Sensing Testing

To examine the impact of varying PLLA and Col ratios on electrical output and strain capacity, we investigated PLLA:Col ratios of 9:1, 8:2, 7:3, 6:4, and 5:5. The optical images of d-PLLA/Col before and after stretching and at the point of fracture are shown in Figure 2a. The mechanical properties of the films with different ratios, including the stress–strain curves and Young's moduli, are shown in **Figure** 3b,c, respectively. Upon the incorporation of Col, the strain of the films was enhanced, and the ductility improved with increasing Col content. However, once the PLLA/Col ratio reached 8:2, the strain capacity approached saturation, with minimal changes observed in the stress–strain curve. Additionally, Young's modulus decreased as the Col doping ratio increased, demonstrating the following values: d-PLLA: 64.9 MPa; d-PLLA/Col (9:1): 37.5 MPa; d-PLLA/Col (8:2): 3.6 MPa; d-PLLA/Col (7:3): 2.8 MPa; d-PLLA/Col (6:4): 2.3 MPa; and d-PLLA/Col (5:5): 2.1 MPa. The improved ductility of the composite films enables a better conformance to the curves of the human body, thereby expanding their potential applications. This enhancement also contributes to greater comfort by reducing

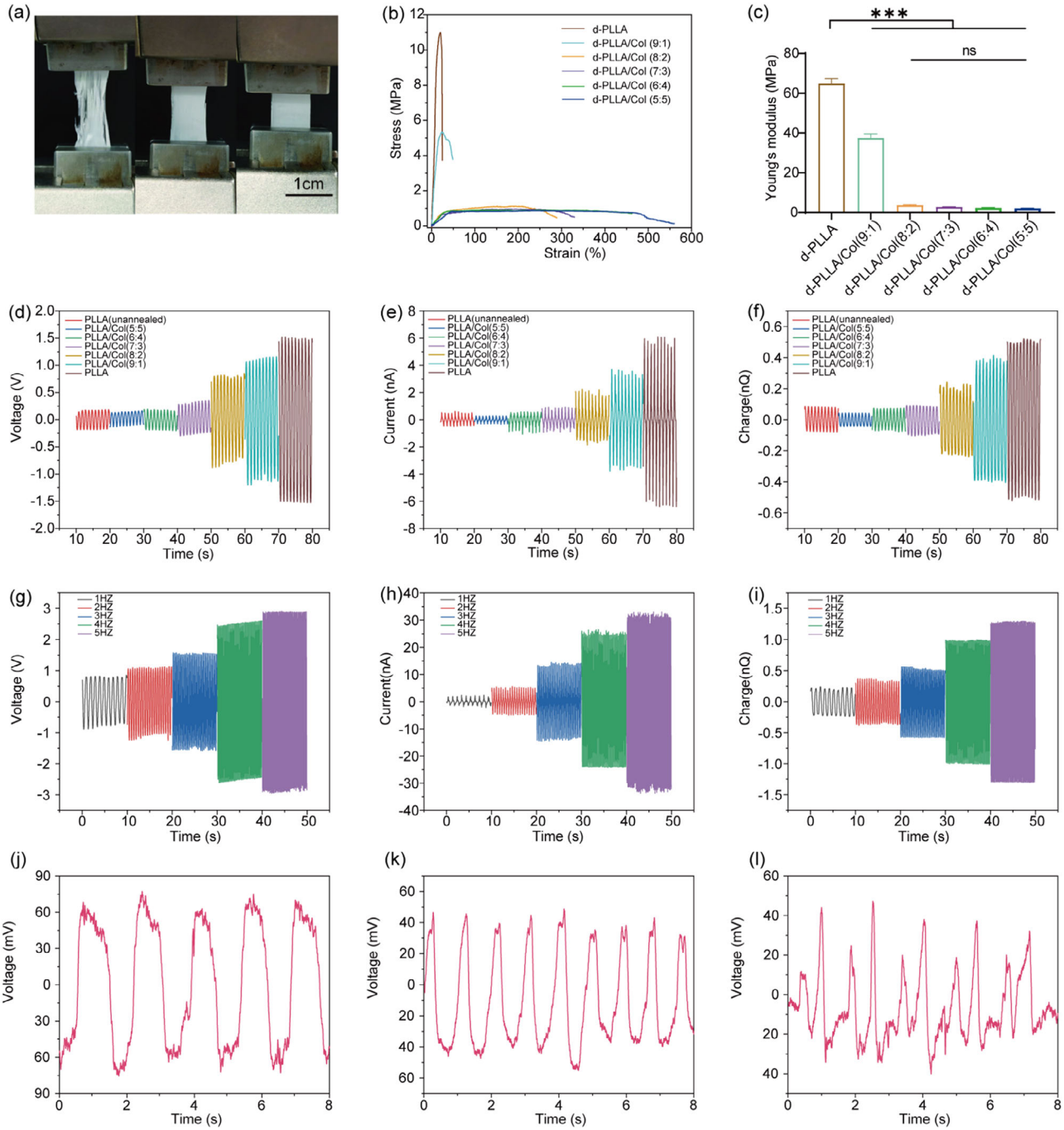

Figure 3. a) Photograph of the tensile test of the composite film. From left to right: the fracture point, stretching process, and starting state. b) Stress–strain curves of the composite films. c) Young's modulus of the composite films ($n = 3$ independent samples. $^{*}p < 0.05$, $^{**}p < 0.01$, and $^{***}p < 0.001$. All statistical analyses were performed by one-way ANOVA. Data are presented as mean ± S.E.M.). d) Output voltage of the composite films. e) Output current of the composite films. f) Output charge of the composite films. g) Output voltage of d-PLLA/Col (8:2) versus the frequency. h) Output current of d-PLLA/Col (8:2) versus the frequency. i) Output charge of d-PLLA/Col (8:2) versus the frequency. j) Output signals during finger bending. k) Output signals during wrist bending. l) Output signals during swallowing.

the friction and discomfort between the device and the skin.[35] Moreover, the decreased Young's modulus indicates that the material is softer and more flexible, allowing the sensors to respond more sensitively to changes in body movements and physiology. This results in more accurate and reliable data collection while distributing pressure more evenly when applied to wounds and minimizing irritation and stress concentrations, which ultimately facilitates a faster and more comfortable healing process. The specific electrical outputs are shown in Figure 3d–f. The unannealed d-PLLA generated negligible piezoelectric

signals, which is consistent with previous reports. d-PLLA exhibited outputs of ≈3.1 V, 12.1 nA, and 1.1 nC. However, upon the addition of Col nanofibers, a reduction in electrical output was observed: d-PLLA/Col (9:1) produced ≈2.3 V, 6.9 nA, and 0.79 nC; d-PLLA/Col (8:2) yielded ≈1.7 V, 4.1 nA, and 0.45 nC; and d-PLLA/Col (7:3) showed a significant decrease to ≈0.56 V, 1.7 nA, and 0.18 nC, producing only a weak electrical signal as the Col content increased. Figure S8 (Supporting Information) shows the electrical signals of some body movements for d-PLLA/Col (7:3). No effective signal could be transmitted at this ratio. Based on these results, d-PLLA/Col (8:2) was determined to be most suitable for maximizing the strain while reducing the Young's modulus of the composite film, thus ensuring sufficient piezoelectricity for enhanced performance in health-monitoring applications. Additionally, the output voltage, current, and charge of the d-PLLA/Col (8:2) thin-film scaffold were evaluated as functions of the frequency. Figure 3g–i illustrates the marked enhancement in the measured electrical signals as the frequency increased from 1 to 5 Hz. This observation indicated that the thin-film scaffold responded effectively to rapid mechanical action, suggesting its potential for use in frequency-responsive devices. To further assess the practical applicability of the d-PLLA/Col (8:2) nanofiber film as a portable wearable sensing device, the output signals were captured during various human activities. The voltage values were used to reflect the performance of the sensors because the open-circuit voltage exhibits a lower susceptibility to interference, resulting in more stable signal outputs.[36] Furthermore, voltage signals can be directly measured using a high-impedance voltmeter or a simple amplification circuit without requiring a charge amplifier, thereby reducing hardware costs.[37] As shown in Figure 3j, the device was mounted on a volunteer's finger, and significant signal variations were observed during finger-bending movements. Similarly, Figure 3k,l show the output signals from the device affixed to the wrist and throat, respectively, showing notable differences during wrist bending and throat swallowing movements. Figure S9 (Supporting Information) shows the output signal of the device affixed to the elbow, which indicates that the sensor is highly sensitive to body movements, confirming its suitability for the real-time monitoring of dynamic physiological states. We further verified several key performance parameters including signal-to-noise ratio calculations, frequency response analysis, and durability. The results are shown in Tables S1 and S2 and Figures S10 and S11 (Supporting Information). We compared the output performance, signal-to-noise ratio, strain capacity, degradability, biocompatibility, and multifunctionality of the investigated systems. The results are summarized in Table S3 (Supporting Information). These comparisons clearly demonstrate the advantages of the strain capacity, degradability, biocompatibility, and multifunctionality of our device. In summary, the experiments demonstrated the capability of d-PLLA/Col (8:2) nanofiber thin-film sensors for real-time transmission, confirming their potential for intelligent monitoring and human health assessment applications.

2.3. Evaluation of Cellular Experiments

The d-PLLA/Col nanofiber film was also capable of generating electrical stimulation driven by high-frequency ultrasound, which is promising for tissue-engineering applications.[38] The ultrasonically driven electrical output, as shown in **Figure 4a**, reveals that the unannealed d-PLLA exhibited a negligible piezoelectric signal, which is consistent with prior theoretical predictions. Upon incorporation of the Col nanofibers, a reduction in the electrical output was observed as d-PLLA/Col (9:1), d-PLLA/Col (8:2), and d-PLLA/Col (7:3) produced values of 0.67, 0.62, and 0.29 V. The remaining composite film ratios generated almost no electrical output. Based on these results, along with the mechanical properties observed from the stress–strain curves, the 8:2 ratio of PLLA to Col was selected for further cellular and animal experiments. This ratio optimized both the mechanical properties of the film and its electrical output under ultrasonic stimulation, thereby enhancing its potential to promote cell growth.

The potential toxicity of nanofibers may be attributed to their small size.[39] Fibers with diameters of >200 nm may exhibit enhanced toxicity because such nanoscale fibers can enter cells via endocytosis and subsequently induce cytotoxic effects.[40] By contrast, the PLLA fibers in this study had diameters exceeding 1000 nm, which prevented direct cellular endocytosis. Additionally, collagen nanofibers immediately transform into hydrogels when they encounter tissue fluids. Furthermore, collagen and PLLA are degraded into biocompatible molecules during metabolism, eliminating concerns regarding degradation-related toxicity. Cell biocompatibility experiments were conducted to systematically evaluate biosafety. Biocompatibility testing was performed using NIH3T3 (fibroblasts), which are key cells involved in wound healing. On day 3, the relative cell viabilities of the PLLA, Col, and PLLA/Col membranes were 91.2%, 98.4%, and 93.0%, respectively (Figure 4b), indicating that these films were noncytotoxic. In vitro cellular experiments were conducted to evaluate the ability of the film scaffolds to induce directional cell growth and promote wound healing. Directed cell growth is crucial for wound healing because it enhances cell migration, tissue mechanical properties, structural integrity, and the local microenvironment. Regulating the directionality of fibroblast growth can increase wound-healing efficiency, shorten healing time, and reduce the risk of complications.[28] The effects of different membrane orientations and ultrasound treatments on the directional growth of fibroblasts were examined. As shown in Figure 4c,d, the control groups (non-ultrasound and ultrasound-treated), along with the PLLA and PLLA/Col membranes, exhibited network patterns with random cell growth and no clear alignment. By contrast, both the non-ultrasound- and ultrasound-treated d-PLLA and d-PLLA/Col membranes promoted an elongated cell morphology, with cells aligned parallel to the fiber orientation.

The distribution of cell orientation (Figure 4e) reveals that both sonicated and untreated d-PLLA and d-PLLA/Col membranes primarily exhibit cell growth angles within ±10°. By contrast, the ultrasound-treated and untreated blank control, PLLA, and PLLA/Col groups exhibited cell angles ranging from 0° to 180°, indicating a lack of directional growth. These findings further validate that the aligned nanofibers are the most effective in guiding directional cell growth, which is consistent with the results of previous studies.

Based on the cell orientation experimental results, four groups, d-PLLA, d-PLLA/US, d-PLLA/Col, and d-PLLA/Col/US,

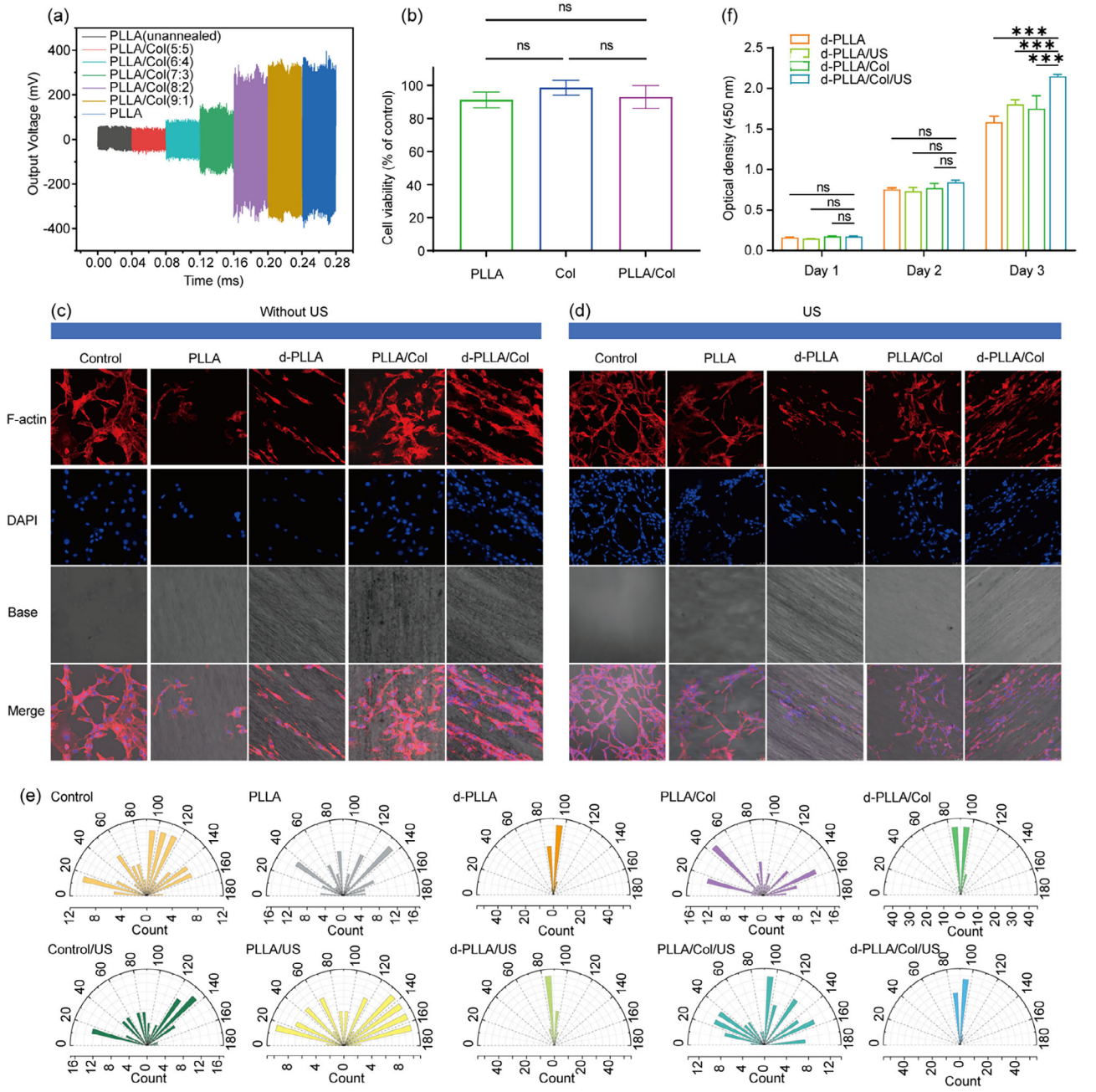

Figure 4. a) Electrical output of ultrasound-driven systems. b) Biocompatibility of PLLA, Col, and PLLA/Col materials ($n = 5$ independent samples. $^{*}p < 0.05$, $^{**}p < 0.01$, and $^{***}p < 0.001$. All statistical analyses were performed by one-way ANOVA. Data are presented as mean ± S.E.M.). c) Cell staining images for the blank control, PLLA, PLLA/Col, d-PLLA, and d-PLLA/Col groups under non-ultrasonication conditions. d) Cell staining images for the blank control, PLLA, PLLA/Col, d-PLLA, and d-PLLA/Col groups under ultrasound conditions. e) Cell growth orientation diagrams for the blank control, PLLA, PLLA/Col, d-PLLA, and d-PLLA/Col groups without and with ultrasound. f) Cell proliferation data for the d-PLLA, d-PLLA/US, d-PLLA/Col, and d-PLLA/Col/US groups ($n = 5$ independent samples. $^{*}p < 0.05$, $^{**}p < 0.01$, and $^{***}p < 0.001$. All statistical analyses were performed by one-way ANOVA. Data are presented as mean ± S.E.M.).

were selected for subsequent cell proliferation experiments. Exogenous electrical stimulation has been shown to accelerate wound edge closure and new tissue formation by altering cell membrane potential, enhancing intercellular signaling, and promoting cell proliferation and migration.[41] The composite film creates an optimal environment for cell growth, supporting proliferation through its physical properties such as stiffness, flexibility, and a collagen fiber arrangement that resembles the natural extracellular matrix (ECM). The proliferation results, presented in Figure 4f, indicate that d-PLLA/Col/US significantly enhanced cell proliferation on day 3 compared with the other groups. This observation is consistent with previous reports that

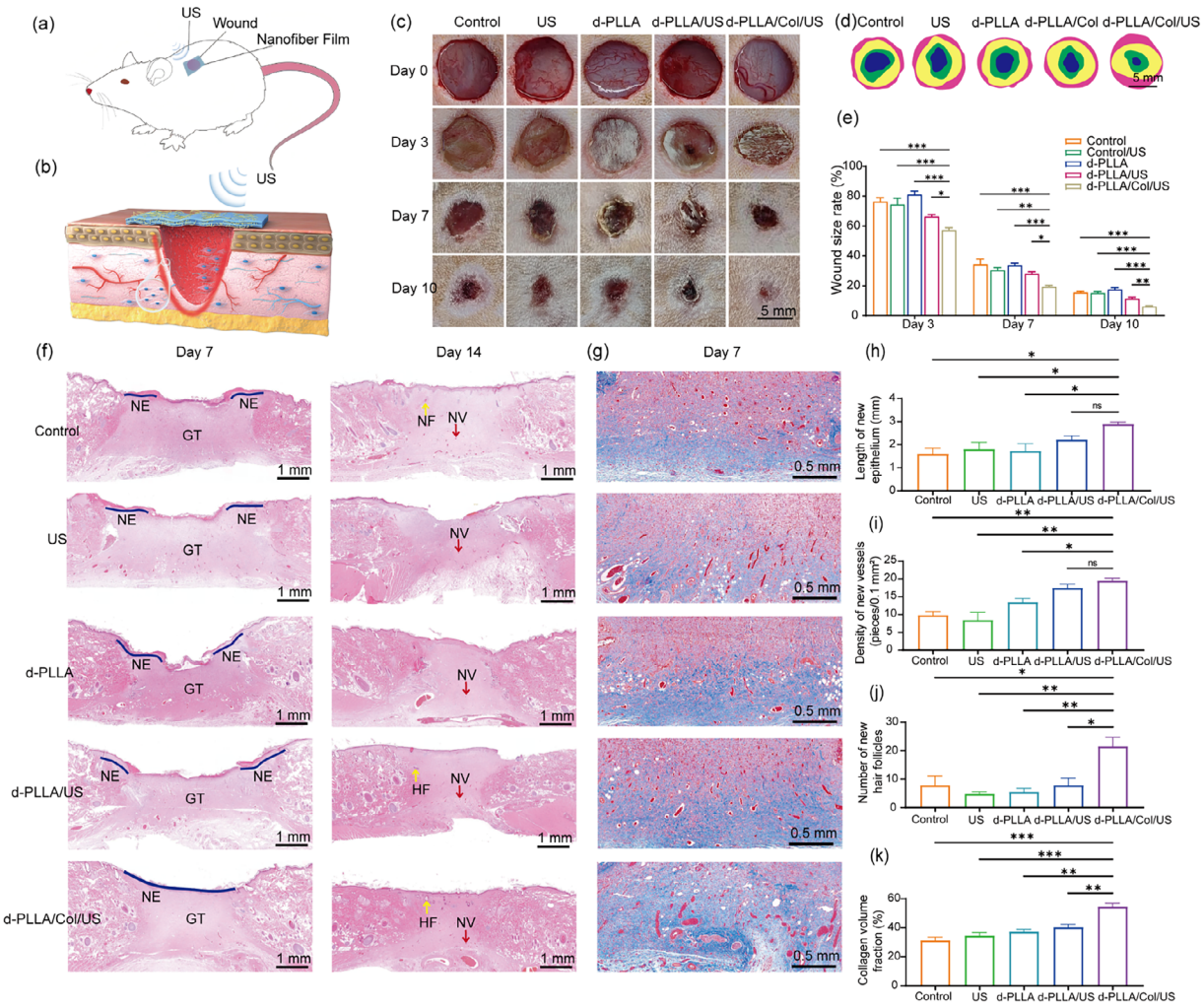

Figure 5. a) Simplified schematic of the in vivo experiment. b) Schematic of wound healing in rats. c) Representative photographs of wound closure over time for different groups. d) Healing traces of skin wound tissues at 10 days postoperatively for each group. e) Quantitative representation of wound sizes at various time points and graphical comparisons between groups. f,g) H&E staining on days 7 and 14 and Masson's trichrome staining on day 14. H&E staining of wound healing tissue show new epithelium (NE), new granulation tissue (GT), new hair follicles (HF), and new vessels (NVs). h) Re-epithelialization length on day 7. i) Number of regenerated blood vessels on day 14. j) Number of regenerated hair follicles on day 14. k) Collagen volume fraction. $n \geq 3$ independent samples. $^{*}p < 0.05$, $^{**}p < 0.01$, and $^{***}p < 0.001$. All statistical analyses were performed by one-way ANOVA. Data are presented as mean ± S.E.M.

ultrasound-induced electrical stimulation combined with recombinant collagen promotes cell proliferation.

2.4. Animal Experimental Validation

To further validate the pro-wound healing efficacy of the d-PLLA/Col films, an in vivo study using rats was conducted. **Figure** 5a,b present an overview of the experimental setup and the rat wound model. Wound healing and new skin formation were monitored by capturing photographs of the entire wound area on days 0, 3, 7, and 10 (Figure 5c). The results shown in Figure 5d,e demonstrate that the d-PLLA/Col/US film-dressing group exhibited the most pronounced therapeutic effect, followed by the d-PLLA/US film-dressing group. By day 3, the d-PLLA/US group showed a 66.4% reduction in wound size, with an average healing rate of 11.2% per day, significantly surpassing those of the blank control group (7.9%), ultrasound control group (8.5%), and d-PLLA control group (6.4%). The d-PLLA/Col/US group displayed the most favorable outcomes, with 57.1% wound closure by day 3 and an average healing rate of 14.3%. By day 7, the wound size in the d-PLLA/Col/US group was reduced to 19.4%, a substantial improvement compared to that in the blank control group (34.3%), ultrasound control group (30.4%), d-PLLA control group (33.7%), and d-PLLA/US group (28.0%). By day 10, the wound area in the d-PLLA/Col/US group had reduced to 6.2% of its original size, indicating near-complete healing, whereas the other control groups exhibited larger wounds with closures of 15.6%, 15.2%, 17.6%, and 11.3% of their original size, respectively. These results clearly demonstrate the superior wound healing efficacy of the d-PLLA/US group compared to that of the blank control, ultrasound (US), and d-PLLA groups.

This enhanced therapeutic effect can be attributed to the beneficial effects of ultrasound-induced electrical stimulation on wound healing. The d-PLLA/Col/US group yielded the most favorable outcomes owing to the microstructural advantages provided by the composite recombinant collagen, which was more effectively aligned with the biomechanical properties of skin wound tissues, thereby improving healing. Moreover, compared with the blank control group, the d-PLLA/Col/US group generated electrical signals in the piezoelectric layer through external ultrasonic stimulation. These signals are transmitted to the surrounding skin tissues via the film dressing, thereby promoting cell migration and re-epithelialization, while also stimulating cell proliferation.[42] Additionally, the incorporation of recombinant collagen endows the structure with enhanced bionic characteristics and mechanical properties, facilitating the creation of an optimal healing environment and accelerating the wound-healing process through synergistic effects.[43]

The skin surrounding the rat wounds was excised for histological analysis using H&E staining on days 7 and 14, and Masson staining on day 7. The results are shown in Figures 5f,g. Changes in wound healing were first observed by H&E staining on days 7 and 14. On postoperative day 7, the wound was in the proliferative phase, characterized by fibroblast migration to the injury site and active re-epithelialization (Figure 5h). Notably, the d-PLLA/Col/US group demonstrated the highest degree of re-epithelialization, with a new epithelial length of ≈2.87 mm, significantly surpassing those of the blank control (1.58 mm), ultrasound (1.78 mm), and d-PLLA (1.7 mm) groups. By day 14, complete re-epithelialization was observed in the d-PLLA/Col/US group along with the highest level of vascular regeneration (Figure 5i). The density of new blood vessels in this group reached 19.33 vessels/0.1 mm^2, which was significantly higher than the blank control (9.67 vessels/0.1 mm^2), ultrasound (8.33 vessels/0.1 mm^2), and d-PLLA (13.33 vessels/0.1 mm^2) groups. Additionally, the d-PLLA/Col/US group exhibited the highest number of regenerated hair follicles on day 14, with 21.33 follicles, significantly surpassing the blank control (7.67 follicles), ultrasound (4.67 follicles), d-PLLA (5.33 follicles), and d-PLLA/US (7.67 follicles) groups (Figure 5j). These results underscore the potent therapeutic effects of d-PLLA/Col/US on skin regeneration.

Collagen synthesis, an indicator of fibroblast migration and skin remodeling, was also assessed. As shown in Figure 5g, the d-PLLA/Col/US group exhibited significantly higher collagen synthesis than the control group. Figure 5k shows that the d-PLLA/Col/US group had the highest collagen deposition, with a collagen volume fraction of 54%, which was markedly higher than that of the other groups. This suggests that the inclusion of recombinant collagen combined with electrical stimulation generated by the piezoelectric effect effectively enhanced collagen synthesis and fibroblast migration into the wound, thereby promoting more efficient wound healing.

3. Conclusion

We successfully developed a flexible and stretchable piezoelectric film based on PLLA and recombinant humanized type I collagen with a homogeneous composite achieved through electrostatic spinning. The composite films exhibited outstanding physicochemical properties, including favorable morphologies, electrical outputs, and mechanical strengths. These properties allow it to accommodate low-frequency tissue deformation or activity, thus validating its ability for sensing and monitoring. Driven by high-frequency ultrasound, biocompatibility assessments and in vitro cell proliferation tests demonstrated the ability of the material to promote targeted cell growth and proliferation. Additionally, in vivo experiments using a rat skin wound model highlighted the synergistic effects of the composite film in enhancing wound healing, thereby highlighting its therapeutic potential.

The significance of this study can be summarized via two main aspects. First, the proposed system overcame the performance limitations of traditional biological piezoelectric materials. Although traditional biodegradable piezoelectric PLLA possesses excellent piezoelectric properties, it has a high Young's modulus and low elongation at break, resulting in a mechanical mismatch with biological tissues. We achieved a directionally aligned fiber-interpenetrating network using a composite strategy of recombinant human-derived type I collagen (Col I) and PLLA to optimize the mechanical properties. The Young's modulus of the composite film was reduced to ≈3.6 MPa, and the elongation at break increased to 200–250%, achieving the coexistence of high piezoelectricity and flexibility. Second, the incorporation of recombinant Col I not only optimized the mechanical properties, but also demonstrated effectiveness and safety during tissue repair. As a major component of the extracellular matrix, it promotes cell adhesion and proliferation, thereby expanding the scope of applications of biological piezoelectric materials. Recombinant Col I exhibits excellent biological characteristics and pro-proliferative capacity while avoiding the risks associated with animal-derived collagen proteins, such as immune rejection and pathogen infection. Furthermore, this study achieved multifunctional applications in both wound healing and health monitoring. The proposed material system integrates wound repair treatment and monitoring functions. The excellent flexibility and stretchability of the composite piezoelectric film enable its adaptation to low-frequency tissue deformation or movement, suggesting its promising potential in wearable sensing applications.

4. Experimental Section

Materials: PLLA (characteristic viscosity 1.2–1.5 dL g^{-1}) was obtained from Esunmed, while recombinant collagen CF-1552 was supplied by Shaanxi Giant Biotechnology Co. Ltd. Hexafluoroisopropanol ($C_3H_2F_6O$) was purchased from Aladdin, and n-(3-Dimethylaminopropyl)-N-ethylcarbodiimide (EDC) and N-Hydroxysuccinimide (NHS) were acquired from MACKLIN.

Preparation of Nanofiber Film Scaffolds: Piezoelectric PLLA nanofiber films were fabricated via electrostatic spinning. A 20% PLLA solution was dissolved in hexafluoroisopropanol and electrospun at a flow rate of 0.8 mL h^{-1} through a 22-gauge needle. Voltages of 12 kV were applied to the needle and –3 kV to the collector. The rotating receiver was set at 500–2500 rpm and fiber formation occurred at 30% relative humidity. The films were annealed at 60–120 °C for 8 h, then cooled to room-temperature.

Recombinant collagen (Col) nanofiber films were prepared using a similar electrospinning method. A 20% Col solution was dissolved in 90% acetic acid and spun at a flow rate of 0.2 mL h^{-1} under the same parameters as for PLLA. After spinning, the films were immersed in a 95 wt.% ethanol solution containing 25 mM EDC and 10 mM NHS for 48 h for collagen cross-linking.

The PLLA/Col composite nanofiber films were produced using the double-tube electrospinning method. PLLA and Col solutions were placed on opposite sides of syringe pumps, with flow rates of 0.8 mL h^{-1} for PLLA and 0.2 mL h^{-1} for Col, respectively. The other parameters were identical to those used for PLLA. After spinning, the composite films were subjected to the same cross-linking and annealing treatments as the individual PLLA and Col films, resulting in the final PLLA/Col film scaffolds.

Characterization of Materials: The microstructures of the nanofiber films were examined using a scanning electron microscope (SU8020), and the fiber diameter distribution and orientation were analyzed. Optical images were captured for preliminary morphological assessment and flexibility evaluation. Fourier-transform infrared (FTIR) spectra were obtained using a VERTEX80v spectrometer (Bruker, Karlsruhe, Germany) to analyze the chemical composition and cross-linking status of the films. X-ray diffraction (XRD) analysis was performed to assess the crystallinity of the films. The hydrophilic and water-retention properties were evaluated by measuring the contact angle and swelling rate. For the contact angle test, the films were cut into squares, and water droplets were applied to the surface using a contact angle tester. To determine the swelling rate, dried films were weighed (W_0), then soaked in 1 × PBS at 37 °C for 30 min, dried again, and weighed (W_1). The swelling rate was calculated as $(W_1 - W_0)/W_0 \times 100\%$. The mechanical properties of the nanofiber films were evaluated via tensile testing using an ESM301/Mark-10 tensile testing system (Mark-10 Company, New York, NY, USA).

Sensor Testing: All human research participants experiments were approved by the Committee on Ethics of Beijing Institute of Nanoenergy and Nanosystems (2025016LZ). Informed written consent was obtained from all participants prior to their inclusion in the study.

A conductive spray paint was applied to both sides of the nanofiber membrane to serve as electrodes, after which the membrane was cut into a rectangular shape measuring 2.0 × 1.0 cm. Copper wires were attached to the electrodes on either side and the entire device was sealed with polytetrafluoroethylene (PTFE) tape to form a piezoelectric sensor. The output electrical signal was directly measured using an electrostatic meter (Keithley 6517) and an oscilloscope (HDO 6104).

Measurement of the Open-Circuit Output Voltage Under Ultrasound: To evaluate the electrical output characteristics of the nanofiber film under ultrasound, the film was fabricated into a piezoelectric sensor following the procedure outlined in Section 4.4. An oscilloscope (HDO 6104) was connected to both sides of the film using wires, and ultrasound waves with an intensity of 1 W cm^{-2} and a frequency of 1 MHz were applied via an ultrasound probe to induce the piezoelectric effect. The piezoelectric voltage outputs of the films were recorded.

Cell Culture: NIH3T3 cells were used for in vitro assays and cultured in high-glucose DMEM. The medium (Solarbio) was supplemented with 10% fetal bovine serum (FBS, Gibco) and 1% penicillin/streptomycin (GA3502, Genview).

Biocompatibility Evaluation: The cytotoxicity of various films was assessed using the CCK-8 (Solarbio) assay. Prior to cell inoculation, the samples were sterilized with ethanol and UV light. The samples were then immersed in high-glucose DMEM for 72 h. NIH3T3 cells were seeded at a density of 1×10^5 cells in both the material-impregnated and standard high-glucose DMEM media, and cultured for 72 h. Cell viability was evaluated using the CCK-8 assay.

In Vitro Wound Healing Assays—Directed Cell Growth: Following sterilization with ethanol and UV light, the sterile membrane was evenly adhered to a cell culture dish containing PDMS and placed in 24-well plates for the NIH3T3 cell culture. At 12 h, the samples in the well plates were subjected to sonication using an ultrasound physiotherapy instrument at a frequency of 1 MHz and power of 0.5 W cm^{-2} for 3 min daily. After 72 h, the cells were collected for staining and immunofluorescence imaging was performed using a Leica confocal fluorescence microscope (LEICA TCS SP8) to observe directed cell growth.

In Vitro Wound Healing Assays—Cell Proliferation: The samples were sterilized with ethanol and UV light, placed in 24-well plates, and immersed in 1x PBS for 1 h. NIH3T3 cells were cultured in the plates, and sonication of the samples was performed after 12 h of cell culturing, following the sonication parameters described in Section 4.8.1. Sonication was repeated every 24 h, and the cells were collected at 24, 48, and 72 h for the CCK-8 assay. Cell proliferation on the membrane was assessed by measuring absorbance using an enzyme marker (Thermo Fisher Multiskan FC, Milton Freewater, OR, USA).

In Vivo Wound Healing Studies—Film Scaffold Implantation: Six-week-old male SD rats were purchased from Vital River (Beijing, China). All animal experiments were approved by the Committee on Ethics of Beijing Institute of Nanoenergy and Nanosystems (2024007LZ).

Film samples with diameters of 10 mm were sterilized with ethanol and UV light prior to the implantation experiments. The groups were designated as blank control, ultrasound, d-PLLA, d-PLLA/US, and d-PLLA/COL/US, each with six wounds. After anesthetizing the rats, two circular wounds were created on each side of the dorsal midline using a 9 mm skin punch, removing the entire dermal layer. Film samples were placed over the wounds, covered with a non-adhesive gauze, and secured with self-adhesive bandages.

In Vivo Wound Healing Studies—Ultrasound Treatment: Ultrasound treatments were applied to SD rats using an ultrasound physiotherapy instrument set at a frequency of 1 MHz frequency and 0.5 W cm^{-2} power for 10 min daily. Each session consisted of two intervals, separated by 30 min, and conducted five days a week for a duration of two weeks. The rats were anesthetized and covered with Tegaderm dressing (3 M; Tegaderm) to prevent wound contamination during the ultrasound procedure. The rats were positioned using an ultrasound physiotherapy instrument. The animals in the control group, which did not receive ultrasound treatment, were anesthetized for the same duration to maintain consistency. Photographs of the wounds were taken on days 0, 3, 7, 10, and 14, and the wound areas were measured.

Histological Analysis: To assess skin tissue regeneration, wound tissues were collected on days 7 and 14 for histological staining, including Hematoxylin-Eosin (H&E) and Masson's trichrome staining. Parameters such as collagen deposition, epithelial regeneration length, hair follicle regeneration, and vascularization were quantified using ImageJ software.

Statistical Analysis: The statistical significance of the differences was determined by one-way analysis of variance (ANOVA). Data were analyzed as mean ± standard error of mean (S.E.M.) in GraphPad Prism v. 6. All results were replicated at least three times ($n \geq 3$). Image-Pro Plus 6.0, Origin 2019, and GraphPad Prism v. 6 were used for data plotting. $^{*}p < 0.05$, $^{**}p < 0.01$, and $^{***}p < 0.001$ were considered statistically significant.

Supporting Information

Supporting Information is available from the Wiley Online Library or from the author.

Acknowledgements

Y.X., and R.L. contributed equally to this work. This work was supported by National Key Research and Development Program of China (2022YFB3804700), National Natural Science Foundation of China (T2125003, 52203325, 22378330), Beijing Natural Science Foundation (L245015, Z240022), Shanghai "science and technology innovation action plan" experimental animal research project (22140902000), and the Fundamental Research Funds for the Central Universities.

Conflict of Interest

The authors declare no conflict of interest.

Data Availability Statement

The data that support the findings of this study are available from the corresponding author upon reasonable request.

Keywords

electrical stimulation therapy, monitoring, piezoelectric nanofibers, recombinant collagen, stretchability

Received: February 6, 2025
Revised: July 8, 2025
Published online:

[1] Y. Wang, M. Chao, P. Wan, L. Zhang, *Nano Energy* **2020**, *70*, 104560.
[2] S. Wang, J. Xiang, Y. Sun, H. Wang, X. Du, X. Cheng, Z. Du, H. Wang, *Carbohydr. Polym.* **2021**, *261*, 117894.
[3] A. Sultana, S. K. Ghosh, V. Sencadas, T. Zheng, M. J. Higgins, T. R. Middya, D. Mandal, *J. Mater. Chem. B* **2017**, *5*, 7352.
[4] W. Gao, C. Yu, *Adv. Healthcare Mater.* **2021**, *10*, 2101548.
[5] C. Wang, Y. Hu, Y. Liu, Y. Shan, X. Qu, J. Xue, T. He, S. Cheng, H. Zhou, W. Liu, *Adv. Funct. Mater.* **2023**, *33*, 2303696.
[6] J. An, H. Park, Y. H. Jung, S. Min, D. H. Kim, D. J. Joe, S. G. Lee, D. Y. Hyeon, Y. Je, H. S. Seo, *Nano Energy* **2024**, *121*, 109227.
[7] P. Wu, P. Chen, C. Xu, Q. Wang, F. Zhang, K. Yang, W. Jiang, J. Feng, Z. Luo, *Nano Energy* **2022**, *102*, 107707.
[8] H. F. Guo, Z. S. Li, S. W. Dong, W. J. Chen, L. Deng, Y. F. Wang, D. J. Ying, *Colloids Surf., B* **2012**, *96*, 29.
[9] D. Kim, S. A. Han, J. H. Kim, J. H. Lee, S. W. Kim, S. W. Lee, *Adv. Mater.* **2020**, *32*, 1906989.
[10] M. H. Seo, J. Y. Yoo, S. Y. Choi, J. S. Lee, K. W. Choi, C. K. Jeong, K. J. Lee, J. B. Yoon, *ACS Nano* **2017**, *11*, 1520.
[11] M. T. Chorsi, E. J. Curry, H. T. Chorsi, R. Das, J. Baroody, P. K. Purohit, H. Ilies, T. D. Nguyen, *Adv. Mater.* **2019**, *31*, 1802084.
[12] C. K. Jeong, I. Kim, K. I. Park, M. H. Oh, H. Paik, G. T. Hwang, K. No, Y. S. Nam, K. J. Lee, *ACS Nano* **2013**, *7*, 11016.
[13] Y. Bai, H. Meng, Z. Li, Z. L. Wang, *Med Mat* **2024**, *1*, 40.
[14] L. Xu, Q. kun Zhang, Z. Hu, C. Hua, L. Xue, P. Lu, F. Zhang, Y. Zhang, J. Xiong, *Colloids Surf. A* **2025**, *706*, 135813.
[15] Q. Yu, Y. Bai, Z. Li, F. Jiang, R. Luo, Y. Gai, Z. Liu, L. Zhou, Y. Wang, C. Li, *Nano Energy* **2024**, *121*, 109196.
[16] M. Xu, Y. Wen, F. Niu, Q. Yang, C. Xiong, Z. Shi, *Composites, Part A* **2023**, *169*, 107518.
[17] M. Xu, Y. Wen, Z. Shi, C. Xiong, F. Zhu, Q. Yang, *Polymers* **2024**, *16*, 3314.
[18] A. M. El-hadi, A. M. Abd Elbary, *J. Mater. Sci.: Mater. Electron.* **2018**, *29*, 16496.
[19] L. Li, M. Zhang, Z. Wang, Y. Hu, H. Gu, J. Xiong, *Surf. Interfaces* **2024**, *52*, 104907.
[20] R. Das, T. T. Le, B. Schiff, M. T. Chorsi, J. Park, P. Lam, A. Kemerley, A. M. Supran, A. Eshed, N. Luu, *Int. J. Biol. Macromol.* **2022**, *301*, 122270.
[21] Z. Wang, Y. Yang, Y. Gao, Z. Xu, S. Yang, M. Jin, *Int. J. Biol. Macromol.* **2022**, *211*, 400.
[22] T. Liu, J. Hao, H. Lei, Y. Chen, L. Liu, L. Jia, J. Gu, H. Kang, J. Shi, J. He, *Regen. Biomater.* **2024**, *11*, rbae108.
[23] Z. Dong, Q. Liu, X. Han, X. Zhang, X. Wang, C. Hu, X. Li, J. Liang, Y. Chen, Y. Fan, *J. Mater. Chem. B* **2023**, *11*, 6346.
[24] H. Lei, C. Zhu, D. Fan, *Carbohydr. Polym.* **2020**, *239*, 116249.
[25] F. Cheng, D. Song, H. Li, S. K. Ravi, S. C. Tan, *Adv. Funct. Mater.* **2024**, *35*, 2406950.
[26] J. E. Ruiz Rocha, K. R. Moreno Tovar, R. N. Mendoza, S. Gutiérrez Granados, S. Cavaliere, D. Giaume, P. Barboux, J. S. J. Ferrer, *Nanomaterials* **2023**, *13*, 2648.
[27] P. Nitti, N. Gallo, L. Natta, F. Scalera, B. Palazzo, A. Sannino, F. Gervaso, *J. Healthc. Eng.* **2018**, *2018*, 3651480.
[28] L. Wang, L. Mao, F. Qi, X. Li, M. W. Ullah, M. Zhao, Z. Shi, G. Yang, *Chem. Eng. J.* **2021**, *424*, 130563.
[29] C. Tu, S. Jiang, H. Li, S. Yan, *Macromolecules* **2013**, *46*, 5215.
[30] J. F. Tressler, S. Alkoy, R. E. Newnham, *J. Electroceram.* **1998**, *2*, 257.
[31] M. Yan, X. An, S. Duan, Z. Jiang, X. Liu, X. Zhao, Y. Li, *Int. J. Biol. Macromol.* **2022**, *213*, 639.
[32] E. J. Curry, K. Ke, M. T. Chorsi, K. S. Wrobel, A. N. Miller, III, A. Patel, I. Kim, J. Feng, L. Yue, Q. Wu, *Proc. Natl. Acad. Sci. USA* **2018**, *115*, 909.
[33] F. Jiang, Y. Shan, J. Tian, L. Xu, C. Li, F. Yu, X. Cui, C. Wang, Z. Li, K. Ren, *Adv. Mater. Interfaces* **2023**, *10*, 2202474.
[34] J. Ahmed, M. Gultekinoglu, M. Edirisinghe, *Biotechnol. Adv.* **2020**, *41*, 107549.
[35] A. Yu, M. Zhu, C. Chen, Y. Li, H. Cui, S. Liu, Q. Zhao, *Adv. Healthcare Mater.* **2024**, *13*, 2302460.
[36] K. Kim, J. Kim, X. Jiang, T. Kim, *J. Sens.* **2021**, *2021*, 6664200.
[37] J. M. D. Pereira, *IEEE Instrum. Meas. Mag.* **2006**, *9*, 27.
[38] T. Vinikoor, G. K. Dzidotor, T. T. Le, Y. Liu, H. M. Kan, S. Barui, M. T. Chorsi, E. J. Curry, E. Reinhardt, H. Wang, *Nat. Commun.* **2023**, *14*, 6257.
[39] L. Horváth, A. Magrez, B. Schwaller, L. Forró, *Supramolecular Structure and Function 10*, **2011**, pp 133-149.
[40] M. K. Logan, S. D. Irvin, M. Enfrin, H. Arafat, L. F. Dumée, Y. Gibert, *J. Environ. Chem. Eng.* **2023**, *11*, 110727.
[41] R. Luo, Y. Liang, J. Yang, H. Feng, Y. Chen, X. Jiang, Z. Zhang, J. Liu, Y. Bai, J. Xue, *Adv. Mater.* **2023**, *35*, 2208395.
[42] R. Yuan, N. Yang, S. Fan, Y. Huang, D. You, J. Wang, Q. Zhang, C. Chu, Z. Chen, L. Liu, *Small* **2021**, *17*, 2103997.
[43] L. Yang, H. Wu, L. Lu, Q. He, B. Xi, H. Yu, R. Luo, Y. Wang, X. Zhang, *Biomaterials* **2021**, *276*, 121055.